PHYSICAL REVIEW D **94,** 114512 (2016)

Equation of state for SU(3) gauge theory via the energy-momentum tensor under gradient flow

Masakiyo Kitazawa,[1,2,*] Takumi Iritani,[3,†] Masayuki Asakawa,[1,‡] Tetsuo Hatsuda,[3,4,§] and Hiroshi Suzuki[5,‖]

[1]*Department of Physics, Osaka University, Toyonaka, Osaka 560-0043, Japan*
[2]*J-PARC Branch, KEK Theory Center, Institute of Particle and Nuclear Studies, KEK, 203-1, Shirakata, Tokai, Ibaraki 319-1106, Japan*
[3]*Theoretical Research Division, Nishina Center, RIKEN, Wako 351-0198, Japan*
[4]*Kavli IPMU (WPI), The University of Tokyo, Chiba 606-8502, Japan*
[5]*Department of Physics, Kyushu University, 744 Motooka, Nishi-ku, Fukuoka 819-0395, Japan*

(Received 30 October 2016; published 21 December 2016)

The energy density and the pressure of SU(3) gauge theory at finite temperature are studied by direct lattice measurements of the renormalized energy-momentum tensor obtained by the gradient flow. Numerical analyses are carried out with $\beta = 6.287$–7.500 corresponding to the lattice spacing $a = 0.013$–0.061 fm. The spatial (temporal) sizes are chosen to be $N_s = 64$, 96, 128 ($N_\tau = 12$, 16, 20, 22, 24) with the aspect ratio, $5.33 \leq N_s/N_\tau \leq 8$. Double extrapolation, $a \to 0$ (the continuum limit) followed by $t \to 0$ (the zero flow-time limit), is taken using the numerical data. Above the critical temperature, the thermodynamic quantities are obtained with a few percent precision including statistical and systematic errors. The results are in good agreement with previous high-precision data obtained by using the integral method.

DOI: 10.1103/PhysRevD.94.114512

I. INTRODUCTION

Thermodynamic observables in QCD such as the energy density ε and the pressure p as functions of temperature T and baryon chemical potential μ_B provide fundamental information for studying the physics of relativistic heavy-ion collisions and compact stars. Because of their importance, high precision lattice simulations of ε and p in SU(3) gauge theory [1–5] and in full QCD [6,7] on the lattice at finite T have been carried out extensively for the past few decades. In most of these studies the integral method [1] is adopted, where ε and p are obtained by integrating so-called the interaction measure $\Delta \equiv \varepsilon - 3p$ calculated on the lattice.

Recently, a new method to calculate thermodynamic quantities has been proposed [8,9] on the basis of the gradient flow [10–14]. In this method, one makes use of the renormalized energy-momentum tensor (EMT) operator $T_{\mu\nu}$ constructed from the "flowed field" at nonzero flow time t [8]. Once EMT is defined, ε and p can be calculated by simply taking thermal averages at any given temperature,

$$\varepsilon = -\langle T_{44} \rangle, \qquad p = \frac{1}{3}\sum_{i=1}^{3} \langle T_{ii} \rangle. \tag{1}$$

This method has been tested for the thermodynamics of SU(3) gauge theory in Ref. [9] for the first time with $\beta = 6/g_0^2 = 5.89$–6.56 corresponding to the lattice spacing $a = 0.041$–0.11 fm and the spatial (temporal) size $N_s = 32$ ($N_\tau = 6$, 8, 10). It was found that the ε and p obtained by the gradient flow with small statistics can be comparable to those obtained by the integral method with high statistics. An extension of this method to full QCD has been also formulated [15] and numerical results were reported recently [16,17].

In the present paper, we report an improved analysis of the thermodynamics of SU(3) gauge theory with the gradient flow. Numerical analyses are carried out with $\beta = 6.287$–7.500 corresponding to the lattice spacing $a = 0.013$–0.061 fm. The spatial (temporal) sizes are chosen to be $N_s = 64$, 96, 128 ($N_\tau = 12$, 16, 20, 22, 24) with the aspect ratio $5.33 \leq N_s/N_\tau \leq 8$. The double extrapolation, $a \to 0$ (the continuum limit) followed by $t \to 0$ (the zero flow-time limit), is taken using the data on these fine lattices. We note that such a double limit could not be taken in Ref. [9] due to the coarse lattice. The lattice spacing a required for these analyses has been determined on the basis of the gradient flow (see Ref. [18] and Appendix A 1).

After taking the double limit, the final results of ε and p above the critical temperature T_c reach a few percent precision with both statistical error and systematic errors. The latter errors are associated with the $a \to 0$ and $t \to 0$ extrapolations as well as the scale setting and lambda parameter. Our high precision results based on the gradient flow are found to be in good agreement with the previous high precision results with the integral method.

This paper is organized as follows. In the next section we introduce the gradient flow and the EMT operator used in our study. After describing the setup of numerical

*kitazawa@phys.sci.osaka-u.ac.jp
†takumi.iritani@riken.jp
‡yuki@phys.sci.osaka-u.ac.jp
§thatsuda@riken.jp
‖hsuzuki@phys.kyushu-u.ac.jp

simulations in Sec. III, the numerical results are presented in Sec. IV. The last section is devoted to a short summary. In the Appendix, the analyses of the lattice spacing and the lambda parameter are described in detail.

II. BASIC FORMULATION

A. Yang-Mills gradient flow

Let us first recapitulate the essential features of the Yang-Mills gradient flow [10] and its application to define the renormalized EMT [8].

The gradient flow of the Yang-Mills field is generated by the differential equation with a flow time t, which has a dimension of inverse mass squared,

$$\frac{dA_\mu(t,x)}{dt} = -g_0^2 \frac{\delta S_{\rm YM}(t)}{\delta A_\mu(t,x)} = D_\nu G_{\nu\mu}(t,x). \tag{2}$$

Here the Yang-Mills action $S_{\rm YM}(t)$ and the field strength $G_{\mu\nu}(t,x)$ are composed of the flowed field $A_\mu(t,x)$, which is a function of t and the four-dimensional Euclidean coordinate x. Color indices are suppressed for simplicity. The initial condition at $t=0$ is taken to be $A_\mu(0,x) = A_\mu(x)$ with $A_\mu(x)$ being the ordinary gauge field in four-dimensional Euclidean spacetime.

With Eq. (2), the gauge field flows along the steepest descent direction of $S_{\rm YM}(t)$ as t increases. At the tree level, Eq. (2) is rewritten as

$$\frac{dA_\mu}{dt} = \partial_\nu\partial_\nu A_\mu + (\text{gauge dependent terms}), \tag{3}$$

which is a diffusion-type equation. Therefore, the gradient flow for $t>0$ acts as a cooling of the gauge field with the smearing radius $\sqrt{8t}$ in the four-dimensional Euclidean spacetime. In Ref. [19], it is proved in pure gauge theory that all composite operators composed of $A_\mu(t,x)$ take finite values for $t>0$. Also, the idea of the gradient flow can be generalized to gauge theory with fermions [20].

B. EMT from gradient flow

In the present study, we use the EMT defined by the short flow-time expansion [8]. Let us consider a composite local operator $O(t,x)$ defined from the field $A_\mu(t,x)$ at positive flow time $t>0$. The short flow-time expansion [19] asserts that in the small t limit this operator can be written as a superposition of local operators of the original gauge theory at $t=0$ as

$$O(t,x) \underset{t\to 0}{\to} \sum_i c_i(t) O_i^{\rm R}(x), \tag{4}$$

where $O_i^{\rm R}(x)$ in the right-hand side are renormalized operators of the original gauge theory at $t=0$ with the subscript i denoting a set of operators, while $c_i(t)$ are associated c-number coefficients calculable in perturbation theory for small t.

In order to define the EMT using Eq. (4), we consider the short flow-time expansion of dimension-four gauge-invariant operators [8]. In pure gauge theory, there are two such operators;

$$U_{\mu\nu}(t,x) = G^a_{\mu\rho}(t,x)G^a_{\nu\rho}(t,x) - \frac{1}{4}\delta_{\mu\nu}G^a_{\rho\sigma}(t,x)G^a_{\rho\sigma}(t,x), \tag{5}$$

$$E(t,x) = \frac{1}{4}G^a_{\mu\nu}(t,x)G^a_{\mu\nu}(t,x). \tag{6}$$

Since they are gauge invariant, only gauge invariant operators appear in the right-hand side of Eq. (4): Such an operator with dimension-zero is an identity operator, while operators with dimension-four are EMTs $T_{\mu\nu}(x)$. Up to this order, the short flow-time expansion of Eqs. (5) and (6) thus gives[1]

$$U_{\mu\nu}(t,x) = \alpha_U(t)\left[T_{\mu\nu}(x) - \frac{1}{4}\delta_{\mu\nu}T_{\rho\rho}(x)\right] + O(t), \tag{7}$$

$$E(t,x) = \langle E(t,x)\rangle_0 + \alpha_E(t)T_{\rho\rho}(x) + O(t). \tag{8}$$

We normalize EMT so that the vacuum expectation values vanish, $\langle T_{\mu\nu}(x)\rangle_0 = 0$. This determines the coefficient of the unit operator in the right-hand side of Eq. (8) to be $\langle E(t,x)\rangle_0$. The unit operator does not appear in Eq. (7) since $U_{\mu\nu}(t,x)$ is traceless. Contributions from the operators of dimension-six or higher are proportional to t or higher from the dimensional reason, and thus they are suppressed for small t.

Combining relations Eqs. (7) and (8), we have

$$T_{\mu\nu}(x) = \lim_{t\to 0} T_{\mu\nu}(t,x), \tag{9}$$

with

$$T_{\mu\nu}(t,x) = \frac{1}{\alpha_U(t)}U_{\mu\nu}(t,x) + \frac{\delta_{\mu\nu}}{4\alpha_E(t)}[E(t,x) - \langle E(t,x)\rangle_0]. \tag{10}$$

The coefficients $\alpha_U(t)$ and $\alpha_E(t)$ are calculated perturbatively in the $\overline{\rm MS}$ scheme in Ref. [8],

$$\alpha_U(t) = \bar{g}(1/\sqrt{8t})^2[1 + 2b_0\bar{s}_1\bar{g}(1/\sqrt{8t})^2 + O(\bar{g}^4)], \tag{11}$$

$$\alpha_E(t) = \frac{1}{2b_0}[1 + 2b_0\bar{s}_2\bar{g}(1/\sqrt{8t})^2 + O(\bar{g}^4)], \tag{12}$$

[1]This useful combination was first given in Ref. [21].

where $\bar{g}(q)$ denotes the running gauge coupling in the $\overline{\mathrm{MS}}$ scheme with $q = 1/\sqrt{8t}$ and

$$\bar{s}_1 = \frac{7}{22} + \frac{1}{2}\gamma_E - \ln 2 \simeq -0.08635752993, \quad (13)$$

$$\bar{s}_2 = \frac{21}{44} - \frac{b_1}{2b_0^2} = \frac{27}{484} \simeq 0.05578512397, \quad (14)$$

with $b_0 = \frac{1}{(4\pi)^2}\frac{11}{3}N_c$, $b_1 = \frac{1}{(4\pi)^4}\frac{34}{3}N_c^2$ with $N_c = 3$.

We note here that (i) the right-hand side of Eq. (9) is independent of the regularization because of its UV finiteness, so that one can take, e.g., the lattice regularization scheme, and (ii) the small t expansion of $U_{\mu\nu}(t,x)$ and $E(t,x)$ implies

$$T_{\mu\nu}(t,x) = T_{\mu\nu}(x) + \mathcal{O}(t). \quad (15)$$

C. Energy density and pressure on the lattice

The thermodynamic quantities are obtained from the expectation values of diagonal elements of the EMT as in Eq. (1). A combination of ε and p called the interaction measure Δ is related to the trace of the EMT (the trace anomaly):

$$\Delta = \varepsilon - 3p = -\langle T_{\mu\mu}(x)\rangle. \quad (16)$$

Also, the entropy density s at zero chemical potential is given by ε and p as

$$sT = \varepsilon + p = -\langle T_{44}(x)\rangle + \frac{1}{3}\sum_{i=1}^{3}\langle T_{ii}(x)\rangle. \quad (17)$$

In the practical numerical analysis, we calculate Eq. (10) on a flowed gauge field with $t > 0$. With finite a, the lattice gauge field has to be smeared by the gradient flow sufficiently to suppress the lattice discretization effect. Since the smearing length of the gradient flow is given by $\sqrt{8t}$, this condition requires $\sqrt{8t} \gtrsim a$. On the other hand, the value of $\sqrt{8t}$ has to be small enough compared with half the temporal extent of the lattice, $1/(2T)$, so that the smearing by the gradient flow does not feel the periodic boundary condition. From these requirements, the measurement has to be performed in the range

$$a \lesssim \sqrt{8t} \lesssim \frac{1}{2T}. \quad (18)$$

When Eq. (10) shows approximate linear dependence as shown in Eq. (15) in a range of t given by Eq. (18), one can take the small t limit and obtain Eq. (9). The linear dependence Eq. (15) can also be violated for large t when the perturbative results of the coefficients in Eqs. (11) and (12) are no longer applicable. This happens when $\sqrt{8t}$ approaches the lambda parameter $\Lambda_{\overline{\mathrm{MS}}}$.

For the measurement of Δ, we have to calculate $\langle E(t,x)\rangle_0$ to carry out vacuum subtraction. This means that the numerical analysis for vacuum configuration is needed in addition to $T > 0$ simulation. On the other hand, the analysis of sT, which depends only on the traceless part, does not require the vacuum subtraction and hence can be performed solely with a nonzero T simulation. This is an advantage of our method compared with the integral method.[2]

III. SIMULATION SETUP

We have performed numerical simulations of SU(3) gauge theory on four-dimensional Euclidean lattices. We considered the Wilson plaquette gauge action under the periodic boundary condition with several different values of $\beta = 6/g_0^2$ with g_0 being the bare coupling constant. Gauge configurations are generated by the pseudo-heat-bath algorithm with the over-relaxation, mixed in the ratio of 1:5. We call one pseudo-heat-bath update plus five over-relaxation sweeps as a "Sweep." Each measurement is separated by 200 Sweeps. Statistical errors are then estimated by the jackknife method. The binsize N_{bin} of the jackknife analysis is determined so that the total number of jackknife bins is 50 unless otherwise stated. We have checked that the N_{bin} dependence of the statistical error is not observed with this binsize.

We use the Wilson gauge action for $S_{\mathrm{YM}}(t)$ in the flow equation, Eq. (2). The gradient flow in the t-direction is numerically solved by the third order Runge-Kutta (RK) method [10]. The RK time step is taken to be 0.01 for small t and is increased gradually as t increases. Accumulation errors due to the RK method are found to be more than 2 orders of magnitude smaller than the statistical errors in all the analyses discussed below.

For the operator $U_{\mu\nu}(t,x)$ in Eq. (5) necessary to analyze s/T^3, we use $G^a_{\mu\nu}(t,x)$ written in terms of the clover leaf representation. For $E(t,x)$ in Eq. (6) necessary to analyze Δ/T^4, we use the mixed representation [23,24],

$$E(t,x)_{\mathrm{imp}} = \frac{3}{4}E(t,x)_{\mathrm{clover}} + \frac{1}{4}E(t,x)_{\mathrm{plaq}}, \quad (19)$$

where $E(t,x)_{\mathrm{clover}}$ is constructed from the clover leaf representation of $G^a_{\mu\nu}(t,x)$ in Eq. (6), while $E(t,x)_{\mathrm{plaq}}$ is defined as [10]

$$E(t,x)_{\mathrm{plaq}} = \frac{1}{18}P(t,x), \quad (20)$$

[2]An alternative method to analyze sT without vacuum subtraction is recently proposed in Refs. [5,22].

with the plaquette $P(t,x) = 1/(6N_c)\sum_{\mu,\nu}\mathrm{ReTr}\,[U_\mu(t,x)\times U_\nu(t,x+\hat{\mu})U_\mu^\dagger(t,x+\hat{\nu})U_\nu^\dagger(t,x)]$. If the Wilson gauge action is employed for both the gauge action and $S_{\mathrm{YM}}(t)$ in Eq. (2), the $O(a^2)$ discretization errors in $E(t,x)_{\mathrm{imp}}$ are canceled out in the tree level [23].

To specify temperature of a lattice as well as to perform the continuum extrapolation, we need to relate β to the lattice spacing a. For this purpose, we have previously performed measurements of a in the range $6.3 \le \beta \le 7.5$ using the gradient flow [18]. As summarized in the Appendix, we derived a relation between the dimensionless reference scale w_0/a and β as

$$\frac{w_0}{a} = \exp\left(\frac{4\pi^2}{33}\beta - 9.1268 + \frac{41.806}{\beta} - \frac{158.26}{\beta^2}\right), \quad (21)$$

which is applicable in the range $6.3 \le \beta \le 7.4$. The statistical error of Eq. (21) associated with the fitting parameters is less than 0.4%. Topological freezing of the data may also introduce an extra 1% error to this result (see Appendix A 1 for more details). To determine T of a lattice in the unit of T_c, we use the critical coupling after the infinite volume extrapolation $\beta_c = 6.33552(47)$ at $N_\tau = 12$ [25] and Eq. (21), which gives

$$w_0 T_c = 0.25244(17). \quad (22)$$

In the definition of the EMT operator, Eq. (10), we need the running coupling $\bar{g}(q)$ in the $\overline{\mathrm{MS}}$ scheme which appears in the coefficients $\alpha_U(t)$ and $\alpha_E(t)$ given by Eqs. (11) and (12). To obtain $\bar{g}(q)$ at $q = 1/\sqrt{8t}$, we need a functional form of $\bar{g}(q)$ and the relation between the lattice spacing and $\Lambda_{\overline{\mathrm{MS}}}$. We use the iterative formula for four-loop running coupling [26] and

$$w_0\Lambda_{\overline{\mathrm{MS}}} = 0.2154(5)(11). \quad (23)$$

See Appendix A 2 as well as Ref. [18] for more details. Note that topological freezing would introduce an extra 1% error to this result, too.

The simulation parameters are summarized in Tables I and II. We perform the numerical simulations for eight different temperatures in the range $0.93 \le T/T_c \le 2.69$ on the lattice of volume $N_s^3 \times N_\tau$ as summarized in Table I. For each T/T_c, we perform numerical simulations for three different values of N_τ. The value of β, lattice volume $N_s^3 \times N_\tau$ and the number of configurations are shown in the table. The aspect ratios N_s/N_τ of all lattices are within the range $5.33 \le N_s/N_\tau \le 8$. The values of N_τ for two coarse lattices are fixed to $N_\tau = 12$ and 16. The finest lattice has the value of N_τ in the range $N_\tau = 20$–24; because the corresponding vacuum simulation on 128^4 lattice requires a large numerical cost, we make use of a single vacuum simulation for several values of T by changing N_τ.

Since the lattice spacing determined by Eq. (21) has 1% error, the value of T/T_c on each lattice is expected to have a similar-size uncertainty. Also, there is a possible finite volume effect, although it is expected to be small due to our large aspect ratio, $5.33 \le N_s/N_\tau$. These small uncertainties are not considered in the final results of Δ/T^4 and s/T^3 to be shown at the end of this paper.

TABLE I. Simulation parameters $\beta = 6/g_0^2$, $N_s^3 \times N_\tau$ and the number of configurations for nonzero temperature simulations at T/T_c. The * symbol in the far right column shows the set of configurations that the corresponding vacuum simulation ($N_s = N_\tau$) is available.

T/T_c	β	N_s	N_τ	Configurations	Vacuum
0.93	6.287	64	12	2125	*
	6.495	96	16	1645	*
	6.800	128	24	2040	*
1.02	6.349	64	12	2000	*
	6.559	96	16	1600	*
	6.800	128	22	2290	*
1.12	6.418	64	12	1875	*
	6.631	96	16	1580	*
	6.800	128	20	2000	*
1.40	6.582	64	12	2080	*
	6.800	128	16	900	*
	7.117	128	24	2000	*
1.68	6.719	64	12	2000	*
	6.941	96	16	1680	*
	7.117	128	20	2000	*
2.10	6.891	64	12	2250	
	7.117	128	16	840	*
	7.296	128	20	2040	
2.31	7.200	96	16	1490	
	7.376	128	20	2020	
	7.519	128	24	1970	
2.69	7.086	64	12	2000	
	7.317	96	16	1560	
	7.500	128	20	2040	

For the measurement of Δ/T^4, we need the vacuum simulation for vacuum subtraction. We carry out the simulations on $N_\tau = N_s$ lattices corresponding to the temperatures in the range $0.93 \le T/T_c \le 1.68$. The simulation parameters are shown in Table II. The configuration

TABLE II. Parameters for vacuum simulations ($N_s = N_\tau$).

β	$N_{s,\tau}$	Configurations
6.287	64	2125
6.349	64	950
6.418	64	1000
6.582	64	800
6.719	64	1000
6.495	96	840
6.559	96	840
6.631	96	900
6.941	96	837
6.800	128	992
7.117	128	1028

sets whose vacuum subtraction is available are shown by the $*$ symbol in the far right column in Table I.

To obtain the expectation values of the EMT with Eqs. (9) and (10), the double extrapolation $(t,a)\to(0,0)$ has to be taken. To proceed this analysis, we first take the continuum limit, $a\to 0$, with fixed t in physical unit. Since the leading lattice discretization effect on the thermodynamic quantities with the Wilson plaquette gauge action is of order a^2 [1], we take the following parametrization to take the continuum limit:

$$\langle T_{\mu\nu}(t,x)\rangle_{\rm lat} = \langle T_{\mu\nu}(t,x)\rangle_{\rm cont} + \frac{b_{\mu\nu}(t)}{N_\tau^2}. \qquad (24)$$

Here, $\langle T_{\mu\nu}(t,x)\rangle_{\rm lat}$ is the expectation value obtained on the lattice with N_τ. One has to determine $b_{\mu\nu}(t)$ for each t independently. Then, we take $t\to 0$ extrapolation by fitting the continuum extrapolated result,

$$\langle T_{\mu\nu}(t,x)\rangle_{\rm cont} = \langle T_{\mu\nu}(x)\rangle + C_{\mu\nu}t, \qquad (25)$$

according to Eq. (15). $C_{\mu\nu}$ has in principle logarithmic t dependence, but we treat it as a constant in our extrapolation.

IV. NUMERICAL RESULTS

A. $\langle T_{\mu\nu}(t,x)\rangle_{\rm lat}$ and its t and a dependences

We first focus on the result for $T = 1.68T_c$ to see the t and a dependences of the numerical results. Shown in Fig. 1 are the t dependence of $\Delta/T^4 = (\epsilon - 3p)/T^4$ (left) and entropy density $s/T^3 = (\epsilon + p)/T^4$ (right) as functions of tT^2 at fixed temperature, $T/T_c = 1.68$, for three different values of the lattice spacing, $\beta = 6.719$, 6.941 and 7.117 ($a = 0.033$, 0.025 and 0.020 fm). For Δ/T^4, the improved operator in Eq. (19) is adopted. Let us discuss the three regions of t separately: (i) For $0 < \sqrt{8t} \lesssim a$, the lattice discretization effect becomes prominent as discussed in Sec. II C. One finds, particularly in the right panel, that

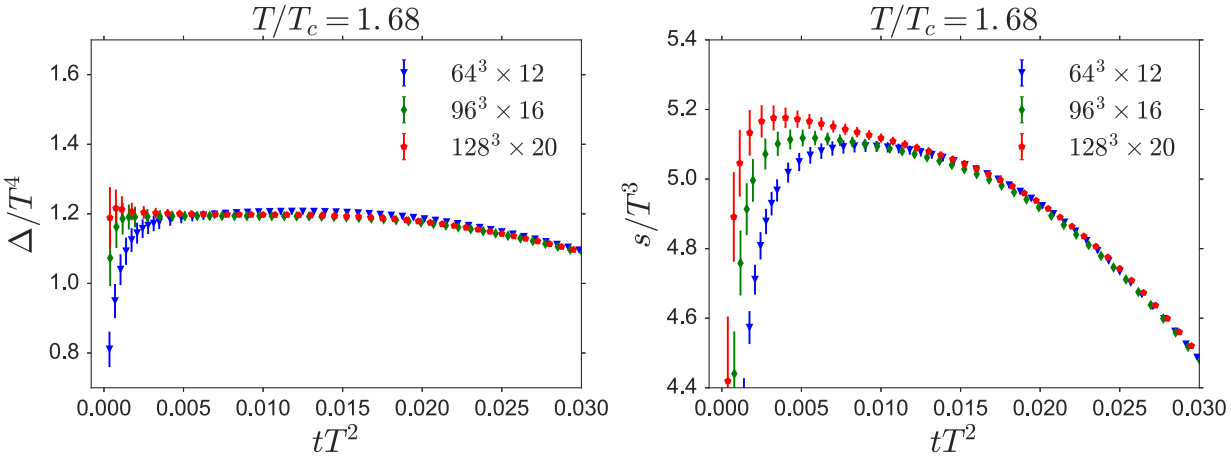

FIG. 1. Flow-time t dependences of trace anomaly $\Delta/T^4 = (\epsilon - 3p)/T^4$ (left) and entropy density $s/T^3 = (\epsilon + p)/T^4$ (right) for $T/T_c = 1.68$ with $N_\tau = 12$, 16 and 20.

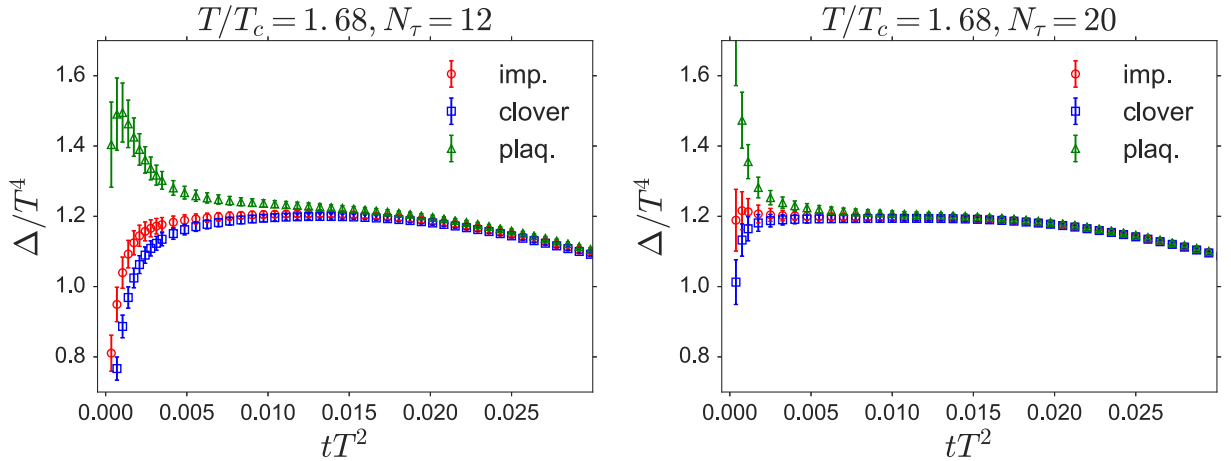

FIG. 2. t dependence of Δ/T^4 for $T/T_c = 1.68$ with $N_\tau = 12$ (left) and $N_\tau = 20$ (right) calculated by different discretizations, $E(t,x)_{\rm imp}$, $E(t,x)_{\rm clover}$ and $E(t,x)_{\rm plaq}$.

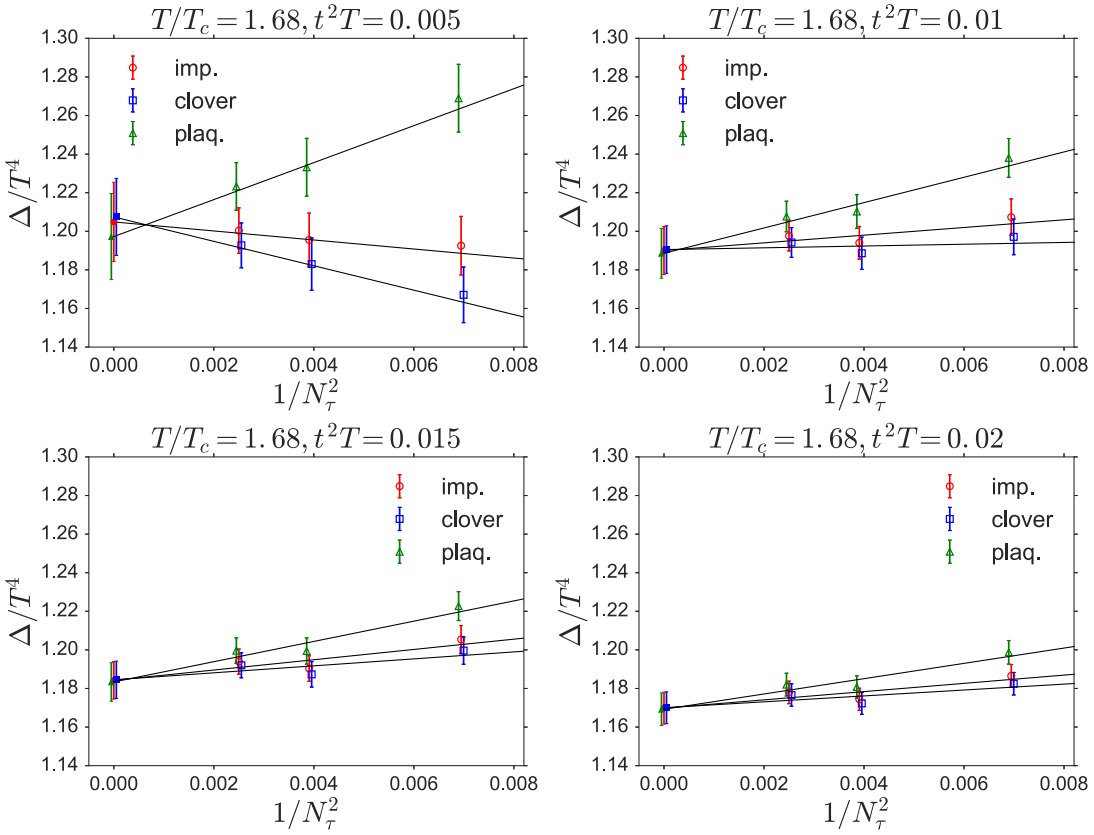

FIG. 3. N_τ dependence of Δ/T^4 at $tT^2 = 0.005$, 0.01, 0.015 and 0.02 together with the result of continuum extrapolation using Eq. (24). The results with three discretizations for $E(t,x)$ are plotted.

this region becomes narrower as a decreases. (ii) For the smallest a in this figure (red points), Δ/T^4 has a plateau and s/T^3 has a linear behavior in the range $0.005 \lesssim tT^2 \lesssim 0.015$ in accordance with Eq. (15). (iii) The deviation from the linear behavior is seen for $tT^2 \gtrsim 0.015$, which is attributed to the over-smearing as discussed in Sec. II C. These considerations indicate that there exists a window of t from which the values of Δ/T^4 and s/T^3 at $t = 0$ can be extracted.

To check the effect of different choices for the operator $E(t,x)$ in Δ/T^4, we compare three cases in Fig. 2, $E(t,x)_{\rm imp}$, $E(t,x)_{\rm clover}$ and $E(t,x)_{\rm plaq}$, for $T/T_c = 1.68$ and $N_\tau = 12$, 20. In both figures, the improved operator, Eq. (19), shows the least discretization error for Δ/T^4.

B. Double extrapolation

Let us now describe the procedure for the double extrapolation $(t,a) \to (0,0)$. As discussed in Sec. III, we first take the continuum limit with t fixed. This extrapolation is taken by fitting the results with three different values of N_τ with Eq. (24). To obtain the values of $\langle T_{\mu\nu}(t,x)\rangle_{\rm lat}$ at the same t for different N_τ, we apply the cubic spline interpolation to the data for each N_τ.

In Figs. 3 and 4, we show the N_τ dependences of Δ/T^4 and s/T^3 at $tT^2 = 0.005$, 0.01, 0.015 and 0.02 together with the result of continuum extrapolation with Eq. (24). In Fig. 3, three results obtained by the different choices for the operator $E(t,x)$ are shown. The value of $\chi^2/{\rm dof}$ is within the range $\chi^2/{\rm dof} \lesssim 2.0$ for $0.005 \le tT^2 \le 0.02$. The error of the continuum extrapolation is estimated by the jackknife analysis. For values of tT^2 smaller than 0.005, the fitting becomes worse particularly for s/T^3. Therefore, in the following, we will use the results only for $0.005 \le tT^2 \le 0.02$. Figure 3 also shows that the continuum extrapolated results with different discretizations for $E(t,x)$ agree with each other.

In Fig. 5, we show the t dependences of Δ/T^4 and s/T^3 after the continuum extrapolation by the black line with the error band together with the data for finite lattice spacings, $N_\tau = 12$, 16 and 20. We make linear t extrapolation by using the continuum extrapolated data for $0.005 \le tT^2 \le 0.02$ according to Eq. (25). We employ three fitting ranges,

Range-1 $0.01 \le tT^2 \le 0.015$,
Range-2 $0.005 \le tT^2 \le 0.015$,
Range-3 $0.01 \le tT^2 \le 0.02$.

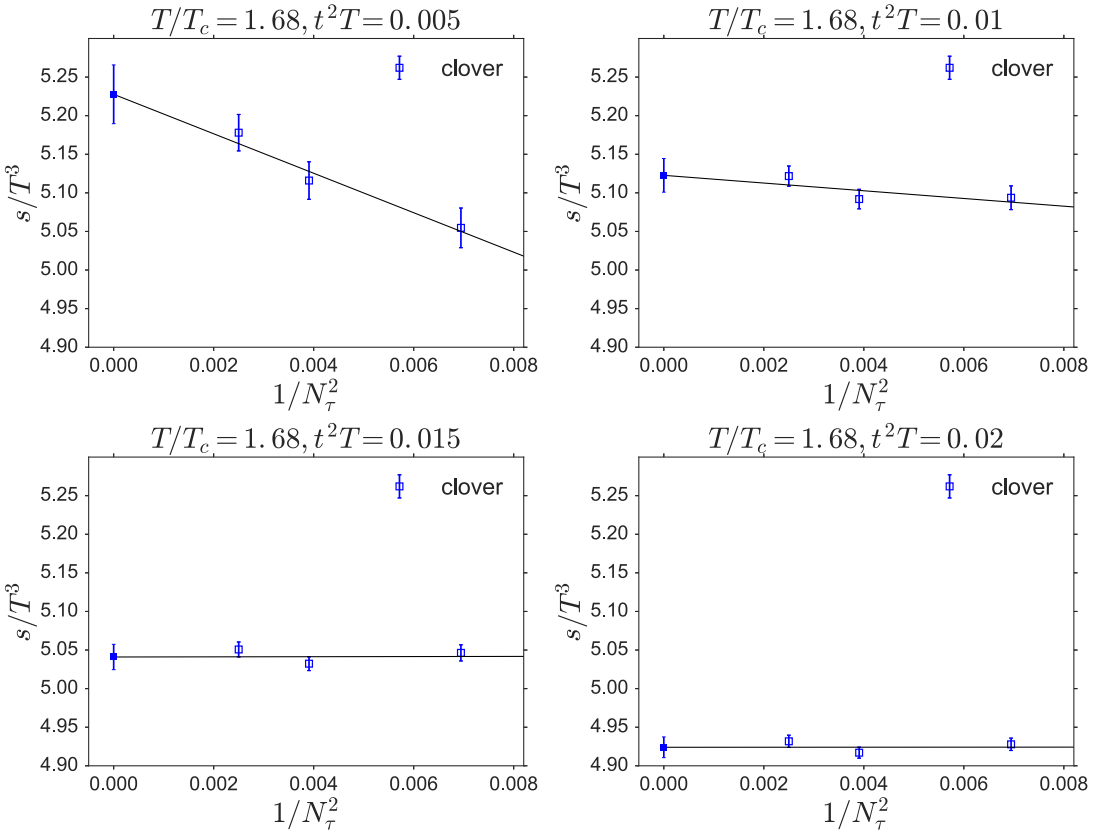

FIG. 4. N_τ dependence of s/T^3 at $tT^2 = 0.005$, 0.01, 0.015 and 0.02 together with the result of continuum extrapolation using Eq. (24).

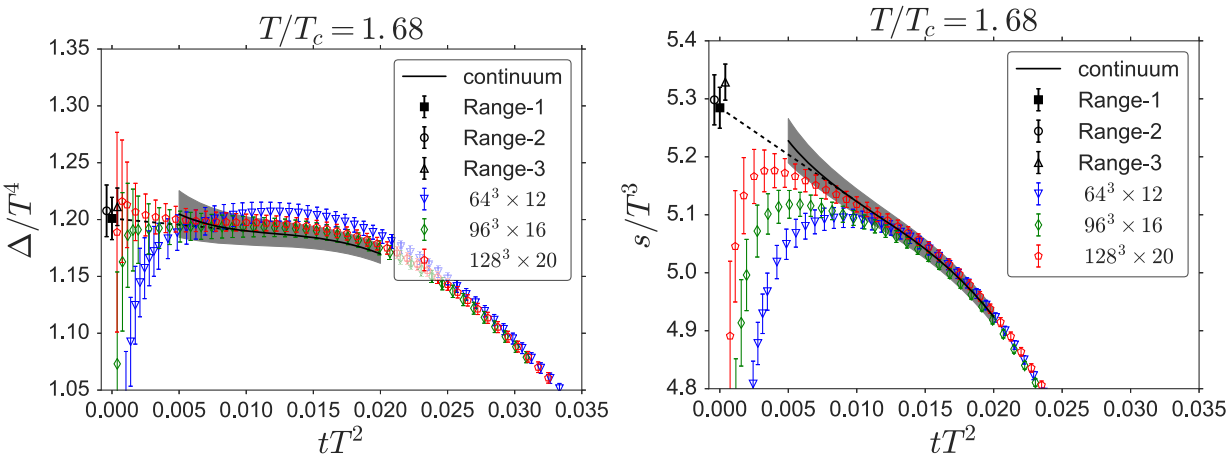

FIG. 5. Results of continuum extrapolation (black band) for Δ/T^4 (left) and s/T^3 (right) as functions of tT^2. The extrapolation to $t = 0$ using the data in Range-1 is shown by the dashed line, and the extrapolated value with the error is given by the filled square at $t = 0$. The extrapolated values with Range-2 and Range-3 are also shown around the origin.

In Fig. 5, the black solid bar at $t = 0$ with a squared symbol denotes the result of the extrapolation with Range-1, while the open circle and triangle symbols denote the results with Range-2 and Range-3, respectively. χ^2/dof in these fittings is smaller than unity. Then, we use the result of Range-1 as a central value, while those of Range-2 and Range-3 are used to estimate the systematic error associated with the fit range.[3]

[3]In our previous exploratory study of Δ/T^4 and s/T^3 in Ref. [9], the continuum limit has been taken, while the flow time was fixed to be $tT^2 = 0.02$. There was no resolution to detect the slope $C_{\mu\nu}$ owing to limited statistics and coarse lattice.

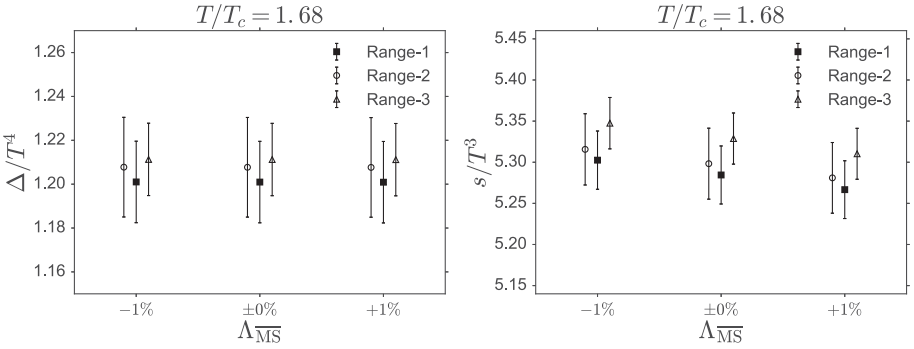

FIG. 6. Systematic errors originated from $\pm 1\%$ of change of $\Lambda_{\overline{\rm MS}}$.

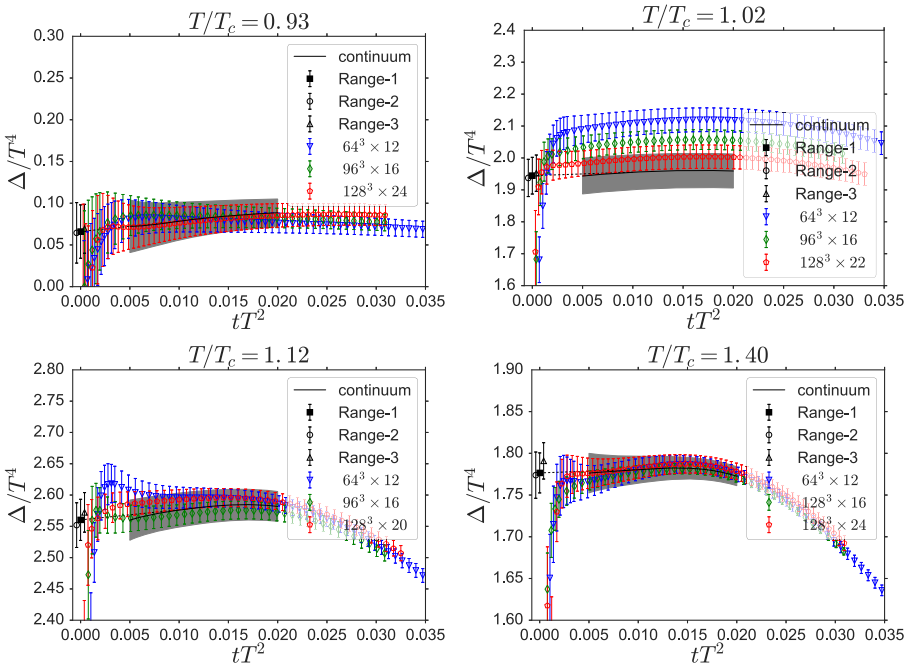

FIG. 7. Similar plots with the left panel of Fig. 5 for different values of T/T_c.

In order to estimate the systematic error from the uncertainly of $a\Lambda_{\overline{\rm MS}}$ discussed in Sec. III, we show the continuum extrapolated results under $\pm 1\%$ change of $a\Lambda_{\overline{\rm MS}}$ in Fig. 6. As the figure shows, the systematic error for Δ/T^4 (s/T^3) is negligible (comparable) to the other statistical and systematic errors.

C. Temperature dependence

The analysis in the previous subsection for $T/T_c = 1.68$ is repeated for all T/T_c listed in Table I. We show the results of these analyses with different values of T/T_c in Fig. 7 for Δ/T^4 and in Fig. 8 for s/T^3. The values of χ^2/dof are within a reasonable range $\chi^2/\mathrm{dof} \lesssim 2$ for all fits with an exception for s/T^3 at $T/T_c = 1.40$. As these figures show, the double extrapolation works rather stably for all T/T_c.

The numerical results after double extrapolation are summarized in Table III. The table shows that Δ/T^4 and s/T^3 are determined within 3% precision including all systematic errors except for those at $T/T_c = 0.93$. Note that we do not have Δ/T^4 for the highest three temperatures owing to the lack of vacuum simulations needed to make vacuum subtraction (see Table I).

Finally, we depict the T/T_c dependences of our Δ/T^4 and s/T^3 in Fig. 9 together with the previous data obtained by the integral method in Refs. [1,4]. By taking into the estimated errors of the previous results, three results are consistent with each other.[4]

[4]We note that s/T^3 recently studied in the shifted boundary method [5,22] also seems to agree.

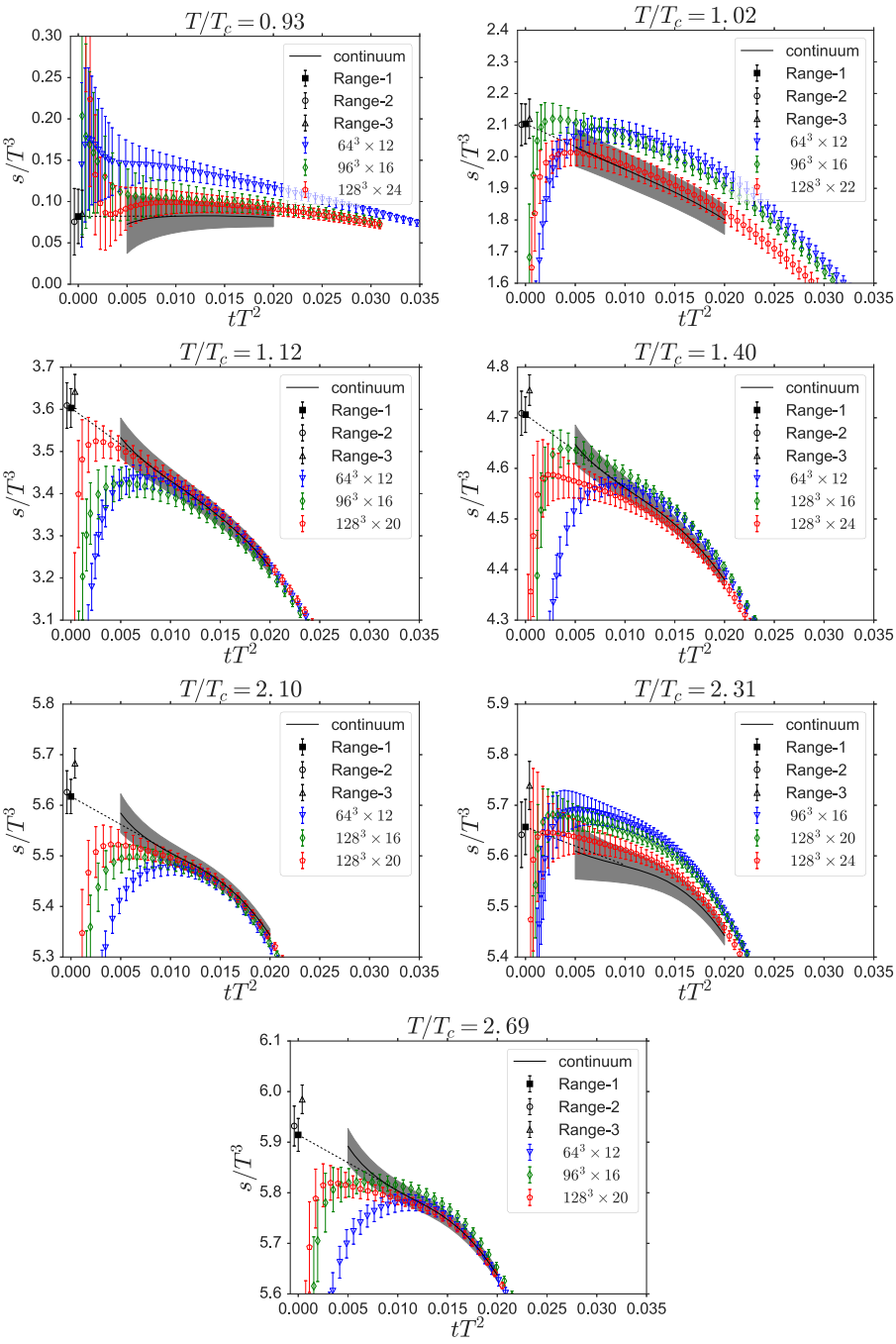

FIG. 8. Similar plots with the right panel of Fig. 5 for different values of T/T_c.

V. SUMMARY

We performed measurements of thermodynamic quantities of the SU(3) Yang-Mills theory from the direct analysis of the expectation value of energy-momentum tensor (EMT), Eq. (9), constructed by the Yang-Mills gradient flow with a flow time t. The numerical simulations with the Wilson plaquette gauge action have been performed at finite temperature with the lattice spacing $a = 0.013$–0.061 fm and the aspect ratio, $5.33 \leq N_s/N_\tau \leq 8$.

Using the lattice data, the double extrapolation ($t \to 0$ after $a \to 0$) has been performed to obtain the interaction measure $\Delta(T)$ and the entropy density $s(T)$ with a few percent precision including statistical and systematic errors. The results agree quite well with the previous high-precision data using the integral method.

The present approach with EMT provides a new tool not only to calculate QCD equation of state accurately but also to study correlation functions and transport coefficients of the quark-gluon plasma with firm theoretical

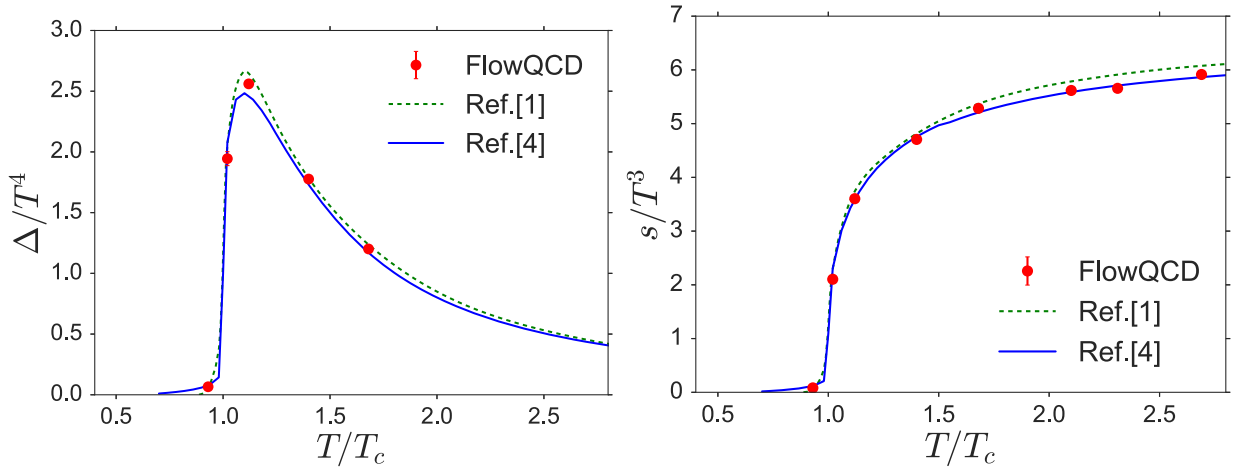

FIG. 9. Temperature dependences of Δ/T^4 and s/T^3 (red circles) together with the previous studies based on the integral method (solid and dashed lines) [1,4]. The error bars of the red circles are smaller than the size of symbols.

basis. The first step along these directions will be reported in the forthcoming paper [27].

ACKNOWLEDGMENTS

The authors thank E. Itou for discussions in the early stage of this study. Numerical simulation for this study was carried out on IBM System Blue Gene Solution at KEK under its Large-Scale Simulation Program (No. 13/14-20, No. 14/15-08, and No. 15/16-15). This work is supported in part by Japan Society for the Promotion of Science KAKENHI Grants No. 24340054, No. 25287046, No. 25287066, No. 25800148, No. 26400272, No. 16H03982 and by RIKEN iTHES Project.

APPENDIX: LATTICE SPACING AND Λ PARAMETER

In this Appendix, we summarize our analysis of the lattice spacing and $\Lambda_{\overline{\rm MS}}$. The numerical data used are those given in Ref. [18]. A possible error originating from the topological freezing is also mentioned.

TABLE III. Summary of the equation of state with statistical and systematic errors. The first error is the statistical one, while the second error shows the systematic error associated with the choice of the fit range. The last error comes from 1% uncertainties of $\Lambda_{\overline{\rm MS}}$ from possible topological freezing. Δ/T^4 at $T/T_c = 2.10$, 2.31 and 2.69 are not available due to the lack of corresponding vacuum configurations.

T/T_c	Δ/T^4	s/T^3
0.93	$0.066(32)(^{+3}_{-2})(0)$	$0.082(33)(^{+3}_{-6})(0)$
1.02	$1.945(57)(^{+8}_{-7})(0)$	$2.104(63)(^{+16}_{-2})(8)$
1.12	$2.560(33)(^{+12}_{-8})(0)$	$3.603(46)(^{+39}_{-0})(13)$
1.40	$1.777(24)(^{+14}_{-3})(0)$	$4.706(35)(^{+49}_{-0})(17)$
1.68	$1.201(19)(^{+10}_{-0})(0)$	$5.285(35)(^{+44}_{-0})(18)$
2.10	—	$5.617(34)(^{+66}_{-0})(18)$
2.31	—	$5.657(55)(^{+82}_{-15})(18)$
2.69	—	$5.914(32)(^{+70}_{-0})(18)$

1. Reference scale and lattice spacing

Numerical simulations of the SU(3) Yang-Mills theory with the Wilson plaquette action were performed on $N_s^4 = 64^4$–128^4 lattices under the periodic boundary condition. The values of $\beta = 6/g_0^2$, N_s and the number of configurations $N_{\rm conf}$ are summarized in the three left columns in Table IV.

We adopt the reference scale w_0 defined by [29]

$$t\frac{d}{dt}t^2\langle E(t)\rangle\big|_{t=w_0^2} = 0.3, \tag{A1}$$

with the operator $E(t)$ constructed by the clover-type representation of the flowed field $G^a_{\mu\nu}$ at time t. We use the Wilson gauge action $S_{\rm YM}$ for the flow equation in Eq. (2), and each measurement is separated by 1000 Sweeps. The values of w_0/a with statistical errors are summarized in the fourth column of Table IV. The lattice spacings in physical unit estimated by $w_0 = 0.1670(10)$ fm [28] are also given in

TABLE IV. Simulation parameters for scale setting, $\beta = 6/g_0^2$, the lattice size N_s, and the number of configurations $N_{\rm conf}$, as well as the numerical results of w_0/a. The lattice spacing a and the physical length $N_s a$ in the physical unit determined from $w_0 = 0.1670(10)$ fm [28] are also shown.

β	N_s	$N_{\rm conf}$	w_0/a	a [fm]	$N_s a$ [fm]
6.3	64	30	2.877(5)	0.058(4)	3.72(22)
6.4	64	100	3.317(4)	0.050(3)	3.22(19)
6.5	64	49	3.797(8)	0.044(3)	2.81(17)
6.6	64	100	4.356(9)	0.038(2)	2.45(15)
6.7	64	30	4.980(23)	0.034(2)	2.15(13)
6.8	64	100	5.652(17)	0.030(2)	1.89(11)
7.0	96	60	7.297(18)	0.023(1)	2.20(13)
7.2	96	53	9.348(66)	0.018(1)	1.71(10)
7.4	128	40	12.084(61)	0.014(1)	1.77(11)

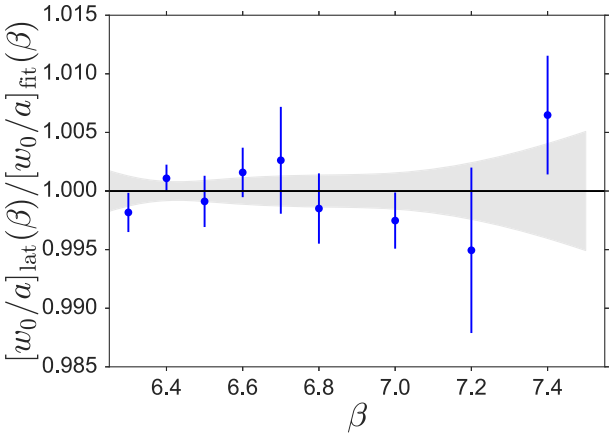

FIG. 10. Result of the three parameter fit of w_0/a in Eq. (A2). The shaded band shows the uncertainties from the fit parameters.

the table together with the physical lattice volume $L = N_s a$. Extra error due to topological freezing is estimated to be about the 1% level as discussed later.[5]

For the parametrization of w_0/a as a function of β, we introduce the fitting function motivated by the one-loop perturbation theory. It provides a reasonable result ($\chi^2/\mathrm{dof} = 1.104$) for nine data points in $6.3 \le \beta \le 7.4$ without overfitting as shown in Fig. 10:

$$\frac{w_0}{a} = \exp\left(\frac{4\pi^2}{33}\beta - 9.1268 + \frac{41.806}{\beta} - \frac{158.26}{\beta^2}\right) \times [1 \pm 0.004(\mathrm{stat})]. \quad \text{(A2)}$$

The difference from other fitting Ansätze (such as polynomial functions as shown in Appendix A in Ref. [18]) is found to be less than 1%. The 0.4% error in Eq. (A2) originates from the statistical errors of w_0/a except for the topological freezing.

For the analysis of w_0/a in Table IV, we have used 30–100 configurations separated by 1000 Sweeps. In order to estimate the effect of the topological freezing on these simulations, we have performed an independent measurement at $\beta = 6.88$ on $N_s^4 = 64^4$ lattice by accumulating $N_{\rm conf} = 1290$ configurations with each measurement separated by 2000 Sweeps. This lattice setup corresponds to the physical size, 64×0.027 fm $\simeq 1.7$ fm, which is comparable to the smallest lattice volume in Table IV. Since observables depend more on the topological sector for smaller spatial volume [33], this analysis would serve as the most severe test for the topological freezing of the data sets in Table IV.

The topological charge is defined by $Q \equiv -\frac{1}{32\pi^2}\epsilon_{\mu\nu\rho\sigma}\int_V d^4x \mathrm{tr}[G_{\mu\nu}(x)G_{\rho\sigma}(x)]$. We take the value of Q at $t = t_0$ defined by $t^2\langle E(t)\rangle|_{t=t_0} = 0.3$ [10]. From this measurement of Q, we find that the autocorrelation length is about 100×2000 Sweeps which is 2–6 times larger than the maximum number of Sweeps used to obtain w_0/a in Table IV. Therefore, there is indeed a danger of the topological freezing. Shown in Fig. 11(a) is a histogram of Q^2 obtained in the simulation. The resultant fluctuation of Q reads $\langle Q^2\rangle = 12.2 \pm 3.2$. Corresponding topological susceptibility is estimated as $\chi a^4 \equiv \langle Q^2\rangle/V = (7.3 \pm 1.9) \times 10^{-7}$, with the error by the jackknife analysis with binsize 100. By using Eq. (A2) and the reference values $w_0 = 0.1670(10)$ fm and $r_0 = 0.49$ fm [28], we find $\chi r_0^4 = 0.084(22)$ which is in the 1.5σ level of agreement with the accurate determination, $\chi r_0^4 = 0.0544(18)$ [34].

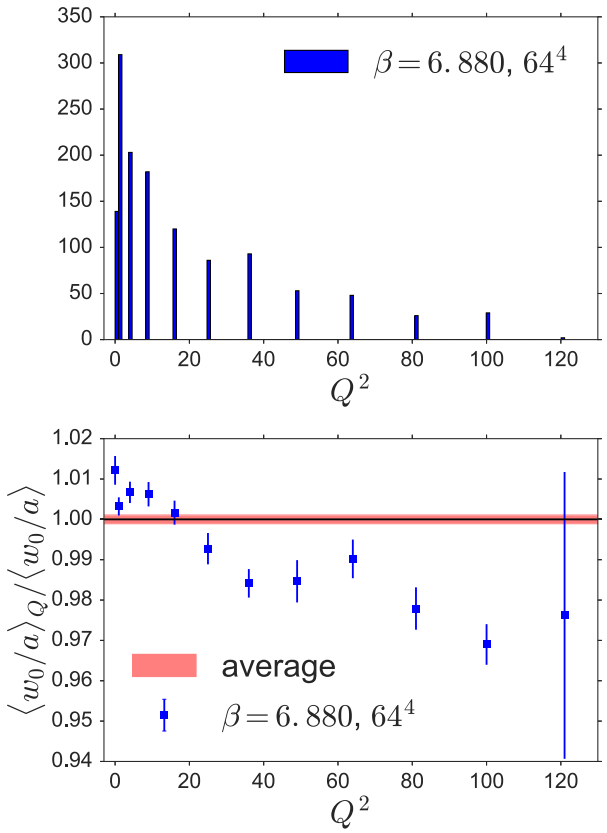

FIG. 11. (a) Histogram of Q^2 for $\beta = 6.88$ and $N_s^4 = 64^4$. (b) The values of w_0/a with fixed Q^2 normalized by the expectation values using all configurations.

In Fig. 11(b), we plot w_0/a at fixed topology, $\langle w_0/a\rangle_Q$, normalized by the expectation value $\langle w_0/a\rangle$ without fixing Q. The red band corresponds to the error of $\langle w_0/a\rangle$ with total configurations. By combining the typical value expected from the topological susceptibility ($|Q| < \sqrt{\langle Q^2\rangle} \lesssim 4$) and the results of Fig. 11, we estimate the effect of the topological freezing is about 1% level.

2. Determination of $\Lambda_{\overline{\rm MS}}$

For the value of $w_0\Lambda_{\overline{\rm MS}}$, we adopt a procedure similar to the one in Ref. [35] for the determination of $r_0\Lambda_{\overline{\rm MS}}$.

[5]See Refs. [30–32] for simulation strategies which are supposed to avoid the topological freezing.

TABLE V. Simulation parameters β and N_s. The plaquette value, w_0/a and $w_0\Lambda_{\overline{\rm MS}}$ using Method I, II and II with Padé approximation. The last row corresponds to the values at the continuum limit obtained from linear extrapolation without using two coarse lattice data at $\beta = 6.3$ and 6.4 (the italic numbers).

				$w_0\Lambda_{\overline{\rm MS}}$		
β	N_s	Plaquette	w_0/a	Method I	Method II	Method II Padé
6.3	64	0.622 420 85(30)	2.877(5)	*0.2017(3)*	*0.2021(3)*	*0.2004(3)*
6.4	64	0.630 632 88(13)	3.317(4)	*0.2046(2)*	*0.2050(2)*	*0.2033(2)*
6.5	64	0.638 361 33(35)	3.797(8)	0.2063(5)	0.2067(5)	0.2051(4)
6.6	64	0.645 669 58(12)	4.356(9)	0.2087(4)	0.2091(4)	0.2075(4)
6.7	64	0.652 608 39(39)	4.980(23)	0.2106(10)	0.2109(10)	0.2095(10)
6.8	64	0.659 215 11(11)	5.652(17)	0.2112(6)	0.2115(6)	0.2101(6)
7.0	96	0.671 556 729(89)	7.297(18)	0.2133(5)	0.2136(5)	0.2123(5)
7.2	96	0.682 891 86(22)	9.348(66)	0.2142(15)	0.2144(15)	0.2132(15)
7.4	128	0.693 365 795(68)	12.084(61)	0.2173(11)	0.2176(11)	0.2164(11)
∞		1	∞	0.2163(5)	0.2165(5)	0.2154(5)
			(χ/dof)	(0.927)	(0.902)	(0.991)

The dimensionless parameter $a\Lambda_{\overline{\rm MS}}$ can be obtained by matching the tadpole improved lattice perturbation theory. The boosted coupling constant $g_\Box$ is defined by

$$g_\Box^2 \equiv g_0^2(a)/u_0^4, \tag{A3}$$

where $u_0^4 \equiv P = \langle {\rm Tr} U_\Box \rangle/3$.

As for the choice of the renormalization scale and the running coupling constant, we take the following two methods:

(i) Method I

$$a\Lambda_{\overline{\rm MS}} = a\mu_* F^{\overline{\rm MS}}(g_{\overline{\rm MS}}(\mu_*)) \tag{A4}$$

at the scale

$$a\mu_* = \exp\left(\frac{t_1^\Box}{2b_0}\right), \tag{A5}$$

and

$$\frac{1}{g^2_{\overline{\rm MS}}(\mu_*)} = \frac{1}{g^2_\Box(a)} + \left(\frac{b_1}{b_0}t_1^\Box - t_2^\Box\right)g_\Box^2(a) + O(g_\Box^4). \tag{A6}$$

(ii) Method II

$$a\Lambda_{\overline{\rm MS}} = a\Lambda_\Box \exp\left(\frac{t_1^\Box}{2b_0}\right), \tag{A7}$$

with

$$a\Lambda_\Box = F^\Box(g_\Box(a)). \tag{A8}$$

This scheme corresponds to choosing a scale at

$$a\mu_= = \exp\left(\frac{t_1^\Box}{2b_0}\right)\frac{F^\Box(g_\Box(a))}{F^{\overline{\rm MS}}(g_\Box(a)} \tag{A9}$$

in Method I.

At the three-loop order, F^S ($S = \Box$, $\overline{\rm MS}$) is expressed as

$$\frac{\Lambda^S}{M} \equiv F^S(g_S(M)) = \exp\left(-\frac{1}{2b_0 g_S^2}\right)(b_0 g_S^2)^{-\frac{b_1}{2b_0}} \times \left(1 + \frac{b_1 + \sqrt{b_1^2 - 4b_0 b_s^S}}{2b_0} g_S^2\right)^{-p_A^S} \times \left(1 + \frac{b_1 + \sqrt{b_1^2 + 4b_0 b_s^S}}{2b_0} g_S^2\right)^{-p_B^S}, \tag{A10}$$

where

$$p_A^S = -\frac{b_1}{4b_0^2} - \frac{b_1^2 - 2b_0 b_2^S}{4b_0^2\sqrt{b_1^2 - 4b_0 b_2^S}}, \tag{A11}$$

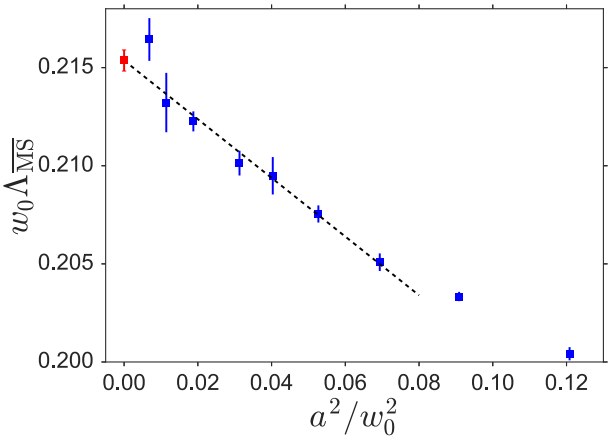

FIG. 12. Values of $w_0\Lambda_{\overline{\rm MS}}$ by the Method II with Padé improvement as a function of lattice spacing a^2. The continuum limit is shown at $a^2/w_0^2 = 0$. The finest lattice data at $\beta = 7.4$ deviates from the fitting line. We note that the continuum extrapolation is consistent within the statistical error without using the result at $\beta = 7.5$.

$$p_B^S = -\frac{b_1}{4b_0^2} + \frac{b_1^2 - 2b_0 b_2^S}{4b_0^2\sqrt{b_1^2 - 4b_0 b_2^S}}. \quad \text{(A12)}$$

In the [1,1] Padé approximation, it leads to

$$F^S_{[1,1]}(g_S(M)) = \exp\left(-\frac{1}{2b_0 g_S^2}\right)\left[\frac{b_0 g_S^2}{1 + (\frac{b_1}{b_0} - \frac{b_2^S}{b_1})g_S^2}\right]^{-\frac{b_1}{2b_0}}. \quad \text{(A13)}$$

In SU(3) Yang-Mills theory, the coefficients are given by

$$b_0 = \frac{11}{(4\pi)^2}, \qquad b_1 = \frac{102}{(4\pi)^4}, \qquad b_2^{\overline{\rm MS}} = \frac{1}{(4\pi)^6}\frac{2857}{2},$$
$$b_2^{\square} = b_2^{\overline{\rm MS}} + b_1 t_1^{\square} - b_0 t_2^{\square}, \quad \text{(A14)}$$

with

$$t_1^{\square} = 0.1348680, \qquad t_2^{\square} = 0.0217565. \quad \text{(A15)}$$

The expectation values of the plaquette, w_0 and $w_0\Lambda_{\overline{\rm MS}}$ with three schemes are summarized in Table V. Following Ref. [35], we adopt Method II with Padé improvement to estimate the central value of $w_0\Lambda_{\overline{\rm MS}}$. The values in the continuum limit are obtained by a linear fit as a function of a^2/w_0^2 without using the coarse results at $\beta = 6.3$ and 6.4 (see Fig. 12). We used the results of the other methods to estimate the systematic error. From this analysis we find

$$w_0\Lambda_{\overline{\rm MS}} = 0.2154(5)(11). \quad \text{(A16)}$$

Note that the topological freezing discussed in Appendix A 1 would introduce another 1% error to this number.

[1] G. Boyd, J. Engels, F. Karsch, E. Laermann, C. Legeland, M. Lutgemeier, and B. Petersson, Thermodynamics of SU(3) lattice gauge theory, Nucl. Phys. **B469**, 419 (1996).

[2] M. Okamoto *et al.* (CP-PACS Collaboration), Equation of state for pure SU(3) gauge theory with renormalization group improved action, Phys. Rev. D **60**, 094510 (1999); Y. Namekawa *et al.* (CP-PACS Collaboration), Thermodynamics of SU(3) gauge theory on anisotropic lattices, Phys. Rev. D **64**, 074507 (2001).

[3] T. Umeda, S. Ejiri, S. Aoki, T. Hatsuda, K. Kanaya, Y. Maezawa, and H. Ohno (WHOT-QCD Collaboration), Fixed scale approach to equation of state in lattice QCD, Phys. Rev. D **79**, 051501 (2009).

[4] S. Borsanyi, G. Endrodi, Z. Fodor, S. D. Katz, and K. K. Szabo, Precision SU(3) lattice thermodynamics for a large temperature range, J. High Energy Phys. 07 (2012) 056.

[5] L. Giusti and M. Pepe, A novel computation of the thermodynamics of the SU(3) Yang-Mills theory, Proc. Sci., LATTICE2015 (**2016**) 211 [arXiv:1511.03710].

[6] S. Borsanyi, Z. Fodor, C. Hoelbling, S. D. Katz, S. Krieg, and K. K. Szabo, Full result for the QCD equation of state with $2 + 1$ flavors, Phys. Lett. B **730**, 99 (2014).

[7] A. Bazavov *et al.* (HotQCD Collaboration), Equation of state in $(2 + 1)$-flavor QCD, Phys. Rev. D **90**, 094503 (2014).

[8] H. Suzuki, Energy-momentum tensor from the Yang-Mills gradient flow, Prog. Theor. Exp. Phys. **2013**, 083B03 (2013); Erratum, Prog. Theor. Exp. Phys. **2015**, 079201 (E) (2015).

[9] M. Asakawa, T. Hatsuda, E. Itou, M. Kitazawa, and H. Suzuki (FlowQCD Collaboration), Thermodynamics of SU(3) gauge theory from gradient flow on the lattice, Phys. Rev. D **90**, 011501 (2014); Erratum, Phys. Rev. D **92**, 059902(E) (2015).

[10] M. Lüscher, Properties and uses of the Wilson flow in lattice QCD, J. High Energy Phys. 08 (2010) 071.

[11] R. Narayanan and H. Neuberger, Infinite N phase transitions in continuum Wilson loop operators, J. High Energy Phys. 03 (2006) 064.

[12] Reviewed in M. Lüscher, Future applications of the Yang-Mills gradient flow in lattice QCD, *Proc. Sci.*, LATTICE2013 (2014) 016 [arXiv:1308.5598].

[13] S. Borsanyi, S. Dürr, Z. Fodor, S. D. Katz, S. Krieg, T. Kurth, S. Mages, A. Schäfer *et al.*, Anisotropy tuning with the Wilson flow, arXiv:1205.0781.

[14] Z. Fodor, K. Holland, J. Kuti, D. Nogradi, and C. H. Wong, The Yang-Mills gradient flow in finite volume, J. High Energy Phys. 11 (2012) 007.

[15] H. Makino and H. Suzuki, Lattice energy-momentum tensor from the Yang-Mills gradient flow-inclusion of fermion fields, Prog. Theor. Exp. Phys. **2014**, 063B02 (2014); Erratum, Prog. Theor. Exp. Phys. **2015**, 079202(E) (2015).

[16] E. Itou, H. Suzuki, Y. Taniguchi, and T. Umeda, $(2 + 1)$-flavor QCD thermodynamics from the gradient flow, *Proc. Sci.*, LATTICE2015 (2016) 303 [arXiv:1511.03009].

[17] Y. Taniguchi, S. Ejiri, R. Iwami, K. Kanaya, M. Kitazawa, H. Suzuki, T. Umeda, and N. Wakabayashi, $\mathrm{Nf} = 2 + 1$ QCD thermodynamics from gradient flow, arXiv:1609.01417.

[18] M. Asakawa, T. Hatsuda, T. Iritani, E. Itou, M. Kitazawa, and H. Suzuki, Determination of reference scales for Wilson gauge action from Yang-Mills gradient flow, arXiv:1503.06516.

[19] M. Lüscher and P. Weisz, Perturbative analysis of the gradient flow in non-Abelian gauge theories, J. High Energy Phys. 02 (2011) 051.

[20] M. Lüscher, Chiral symmetry and the Yang-Mills gradient flow, J. High Energy Phys. 04 (2013) 123.

[21] L. Del Debbio, A. Patella, and A. Rago, Space-time symmetries and the Yang-Mills gradient flow, J. High Energy Phys. 11 (2013) 212.
[22] L. Giusti and H. B. Meyer, Implications of Poincaré symmetry for thermal field theories in finite volume, J. High Energy Phys. 01 (2013) 140.
[23] Z. Fodor, K. Holland, J. Kuti, S. Mondal, D. Nogradi, and C. H. Wong, The lattice gradient flow at tree level and its improvement, J. High Energy Phys. 09 (2014) 018.
[24] N. Kamata and S. Sasaki, Numerical study of tree-level improved lattice gradient flows in pure Yang-Mills theory, arXiv:1609.07115.
[25] M. Shirogane, S. Ejiri, R. Iwami, K. Kanaya, and M. Kitazawa (WHOT-QCD Collaboration), Latent heat at the first order phase transition point of SU(3) gauge theory, Phys. Rev. D **94**, 014506 (2016).
[26] C. Patrignani *et al.* (Particle Data Group Collaboration), Review of particle physics, Chin. Phys. C **40**, 100001 (2016).
[27] M. Kitazawa *et al.* (FlowQCD Collaboration) (to be published).
[28] R. Sommer, Scale setting in lattice QCD, *Proc. Sci.*, LATTICE2013 (2014) 015 [arXiv:1401.3270].
[29] S. Borsanyi, S. Dürr, Z. Fodor, C. Hoelbling, S. D. Katz, S. Krieg, T. Kurth, L. Lellouch, T. Lippert, C. McNeile, and K. K. Szabó, High-precision scale setting in lattice QCD, J. High Energy Phys. 09 (2012) 010.
[30] M. Lüscher and S. Schaefer, Lattice QCD without topology barriers, J. High Energy Phys. 07 (2011) 036.
[31] G. McGlynn and R. D. Mawhinney, Diffusion of topological charge in lattice QCD simulations, Phys. Rev. D **90**, 074502 (2014).
[32] M. G. Endres, R. C. Brower, W. Detmold, K. Orginos, and A. V. Pochinsky, Multiscale Monte Carlo equilibration: Pure Yang-Mills theory, Phys. Rev. D **92**, 114516 (2015).
[33] S. Aoki, H. Fukaya, S. Hashimoto, and T. Onogi, Finite volume QCD at fixed topological charge, Phys. Rev. D **76**, 054508 (2007).
[34] M. Cé, C. Consonni, G. P. Engel, and L. Giusti, Non-Gaussianities in the topological charge distribution of the SU(3) Yang-Mills theory, Phys. Rev. D **92**, 074502 (2015).
[35] M. Göckeler, R. Horsley, A. C. Irving, D. Pleiter, P. E. L. Rakow, G. Schierholz, and H. Stüben, A determination of the Lambda parameter from full lattice QCD, Phys. Rev. D **73**, 014513 (2006).